



Methane, ethane and propane detection using a compact quartz enhanced photoacoustic sensor and a single interband cascade laser

Angelo Sampaolo^{a,b}, Sebastian Csutak^c, Pietro Patimisco^{a,b}, Marilena Giglio^{a,b}, Giansergio Menduni^{a,d}, Vittorio Passaro^d, Frank K. Tittel^b, Max Deffenbaugh^c, Vincenzo Spagnolo^{a,b,*}

^a PolySense Lab - Dipartimento Interateneo di Fisica, Politecnico and University of Bari, Via Amendola 173, Bari, Italy

^b Rice University, Department of Electrical and Computer Engineering, 6100 Main Street, Houston, TX, 77005, USA

^c Aramco Service Company, 16300 Park Row Dr, Houston, TX, 77084 USA

^d Photonics Research Group, Dipartimento di Ingegneria Elettrica e dell'informazione, Politecnico di Bari, Via Orabona 4, Bari, 70126, Italy

ARTICLE INFO

Keywords:

Quartz-enhanced photoacoustic spectroscopy

Gas sensing

Methane

Ethane

Hydrocarbons

Interband

Cascade laser

ABSTRACT

Hydrocarbon detection in the gas phase represents a powerful tool to guide oil exploration and production operations for the oil & gas industry. This application requires highly sensitive, selective and robust spectroscopic techniques. In this work, a quartz-enhanced photoacoustic sensor system designed to detect methane (C1), ethane (C2) and propane (C3), employing a single interband cascade laser emitting in the spectral range 3.342–3.349 μm , is reported. Detection levels in the part-per billion concentration range for C1 and C2 and a few parts per million for C3 were achieved. Measurements at both low and atmospheric pressures were carried out for mixtures simulating typical downhole hydrocarbon concentrations.

1. Introduction

Optical gas sensors typically operate in the near-IR or mid-IR spectral ranges where the strongest absorption features occur. Interband cascade lasers (ICLs) covering the 3–4 μm range [1,2] have led to new opportunities for trace detection of the main hydrocarbon gases [3,4]. Indeed, the fundamental absorption bands of methane (CH_4), ethane (C_2H_6), propane (C_3H_8), ethylene (C_2H_4), propene (C_3H_6) and acetylene (C_2H_2) are located in the $\lambda = 3\text{--}4\text{ }\mu\text{m}$ spectral range [5]. For the petrochemical industry, the monitoring of hydrocarbons such as methane, ethane and propane represents one of the most efficient ways to predict production outputs, estimate reserves and assess raw material quality of source rocks and reservoirs [6].

Among the main spectroscopic detection techniques, Quartz Enhanced Photoacoustic Spectroscopy (QEPAS) has proven to be a perfect candidate for in-situ and real-time trace gas detection, because of an unmatched level of compactness, extremely high sensitivity (down to parts per trillion [7]), immunity to environmental noise and its proven reliability, ruggedness and in-situ operation [8–14]. This technique exploits quartz tuning forks (QTFs) as optoacoustic transducers to convert an acoustic signal into an electrical signal via quartz piezoelectric properties [8,9]. The laser light must be focused between

the QTF prongs and modulated at its resonance frequency (or sub-harmonics). When the laser emission wavelength is resonant with an absorption level of a target gas analyte, the process of periodical heating-relaxation induced by absorption of the modulated light produces pressure waves, i.e. sound. These sound waves produce a deflection of the QTF prongs and the induced strain field is converted into an electrical signal by the QTF. The QEPAS technique does not require any optical detector and is insensitive to the laser wavelength, thereby the same acoustic detection module can operate in any spectral range from UV [15] to THz regime [16,17].

In this work, we report a compact QEPAS sensor prototype for trace gas detection of methane, ethane and propane (also referred in the text as C1, C2, and C3, respectively) by using a single ICL source operating in the spectral range 3.342–3.349 μm . While CH_4 and C_2H_6 detection characterized by well-defined absorption peaks in the ICL operating range was straightforward, propane detection required a preliminary detailed study of the characteristic broadband absorption profiles which merge with the C_2H_6 background signal in the ICL tuning range. A detailed study of gas mixtures containing both C_2H_6 and C_3H_8 allowed us to set up a fitting procedure capable to retrieve both hydrocarbons concentration levels with high precision. Mixtures of C1/C2 were also analyzed to verify that no cross-talk between methane and

* Corresponding author at: PolySense Lab - Dipartimento Interateneo di Fisica, Politecnico and University of Bari, Via Amendola 173, Bari, Italy.

E-mail address: vincenzoluigi.spagnolo@poliba.it (V. Spagnolo).

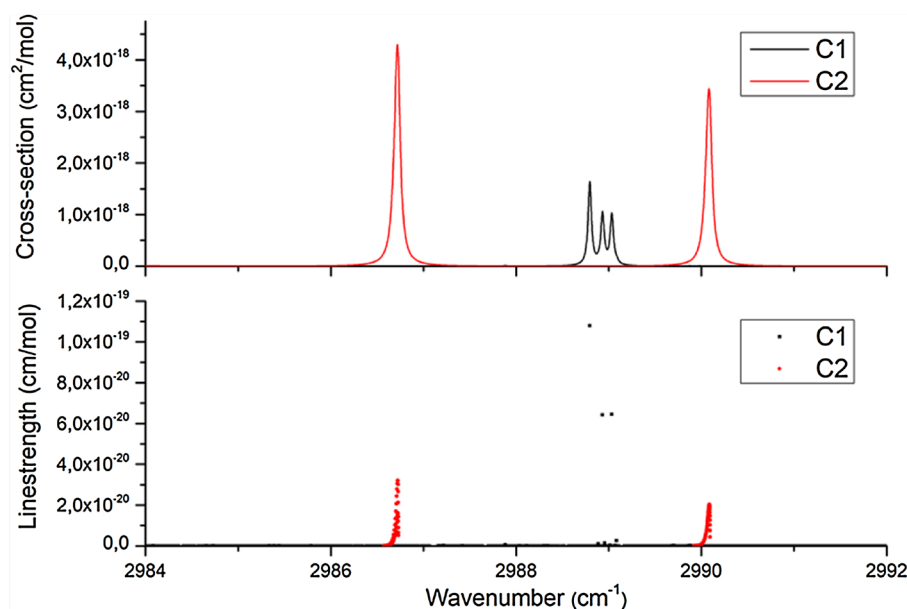


Fig. 1. Top panel: absorption cross-sections at 50 Torr pressure for methane (black curve) and ethane (red curve) in the range 2984–2992 cm^{-1} simulated using the Hitran database [5]. Bottom panel: C1 (black dots) and C2 (red dots) corresponding line strengths. (For interpretation of the references to colour in this figure legend, the reader is referred to the web version of this article).

ethane is observed. For CH_4 and C_2H_6 we reached a detection limit of few parts per billion (ppb)-level, while for C_3H_8 we achieved a few parts per million (ppm) detection limit.

2. Selection of C1 and C2 spectral range for QEPAS operation

As a first step, we identified the spectral region that can be covered with a single ICL source, containing well resolved CH_4 and C_2H_6 absorption features and characterized by absorption cross-sections in the 10^{-18} (cm^2/mol) range.

In Fig. 1 CH_4 and C_2H_6 absorption cross-sections and related line strengths are plotted in the range 2984–2992 cm^{-1} using data from the HITRAN database [5].

These spectra were simulated for pure CH_4 and C_2H_6 at 50 Torr. At this pressure, the absorption line broadening due to collisions is low enough to allow distinguishing the fine structure of the absorption bands. Within a spectral range of 3.5 cm^{-1} there are two Lorentzian-like absorption lines of C_2H_6 , composed by several lines marked in red dots, as shown in the lower panel of Fig. 1, and in the middle three partially merged lines of CH_4 . Even though the line strength of a single CH_4 transition is higher with respect to the two C_2H_6 transitions, the collisional broadening at a pressure of 50 Torr or higher gives rise to two isolated C_2H_6 absorption features with a cross-section larger than the three-fold C1 structures. The spectral separation between the CH_4 three-lines structure and the two C_2H_6 lines guarantees a non-interfering detection of both species.

3. QEPAS sensor configuration

The identification of target lines represented in Fig. 1 led to a specific ICL design commercialized by Nanoplus, with a central emission wavelength of 3345 nm (2989 cm^{-1}). The ICL current dynamic range is $I = 15\text{--}70$ mA and the optimal operating temperature range is from $T = 5^\circ\text{C}$ to $T = 15^\circ\text{C}$. The ICL is mounted in a standard TO66 package equipped with a collimating lens (see Fig. 2). The beam emerging from the lens has a nearly perfect Gaussian power distribution with a diameter of 3 mm. A maximum power of ~ 11 mW was measured at $T = 5^\circ\text{C}$ and $I = 70$ mA with an electric power consumption of 0.273 W.

The high quality of the laser beam allowed operation with a standard 32 kHz QTF (prong spacing of 0.3 mm and length of 3 mm) mounted in an on-beam double tube configuration, constituting the

spectrophone of the QEPAS sensor system. The acoustic detection module (ADM) consists of a cylindrical chamber with gas-in and gas-out connectors and two optical ZnSe windows. The spectrophone is positioned inside the ADM. The employed spectrophone shows a quality factor of $Q = 2100$ at atmospheric pressure and a resonance frequency for the QTF fundamental flexural in-plane mode of $f_0 = 32,741.5$ Hz.

The collimated light exiting the ICL is focused by a ZnSe lens (L1) through the ADM; L1 has a focal length of 7.5 cm and a transmittivity of 95% at 3345 nm. A gas line connects the ADM to the pump on the outlet side and to a pressure controller located at the inlet side. The pressure controller maintains the downstream pressure of the targeted gas mixture into the ADM. The mixtures are generated by flow controllers and a constant water concentration of 1.7% was provided by a Nafion humidifier inserted on one of the gas line. The light exiting from the ADM is re-collimated using a ZnSe lens (L2) and collected by a VIGO detector (model PVI-3TE-3.4) with a detectivity of $7.0 \times 10^{11} \text{ cm}\cdot\text{Hz}^{1/2}\cdot\text{W}^{-1}$, current responsivity $\geq 0.8 \text{ A}\cdot\text{W}^{-1}$ and time constant < 200 ns was used for monitoring the laser power and for alignment purpose. The piezoelectric current generated by the photoacoustic excitation is converted into a voltage signal and amplified by a factor 30 using a transimpedance amplifier (with a feedback resistor of 10 M Ω) and then sent to the Control Electronics Unit (CEU). The CEU is used to determine the main QTF parameters: the electrical resistance R , the quality factor Q , and the resonance frequency f_0 . It is also used to transfer the signal coming from the transimpedance amplifier to a lock-in amplifier. The output analog signal from the lock-in amplifier is then digitalized by a National Instruments DAQ card (USB 6008) connected to a personal computer. LabVIEW-based software acquires the temporal evolution of the QEPAS signal and the response of the pyroelectric detector. All measurements were performed by using an integration time of 100 ms and acquisition time of 300 ms.

4. Sensor calibration for methane detection

We investigated the full ICL dynamic range to retrieve the most convenient experimental conditions for C1-C2 detection in the current scan mode. A mixture of 1000 ppm of $\text{CH}_4:\text{N}_2$ and a mixture of 1000 ppm of $\text{C}_2\text{H}_6:\text{N}_2$ were analyzed. 2f-wavelength modulation (WM) was employed as the detection scheme since it is characterized by a background-free signal [18]. The ICL injected current I was modulated at half of the resonance frequency $f_0/2$ and the QEPAS signal was demodulated at the resonance frequency f_0 (2f-signal). Usually, the

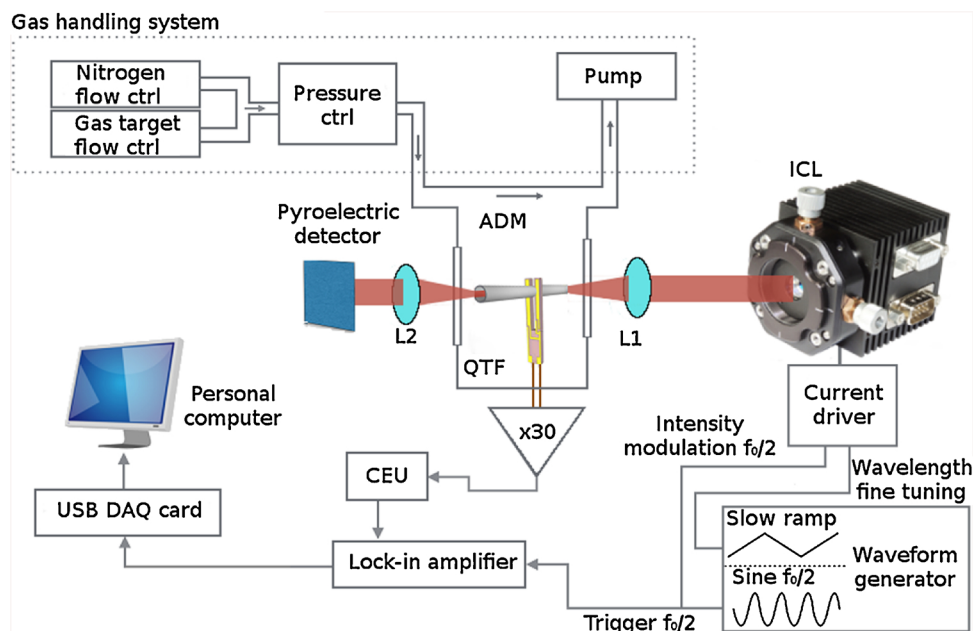


Fig. 2. Schematic of the experimental apparatus. CEU - control-electronic-unit; ADM - acoustic detection module; L1, L2 –ZnSe lenses; ICL – intercascade laser.

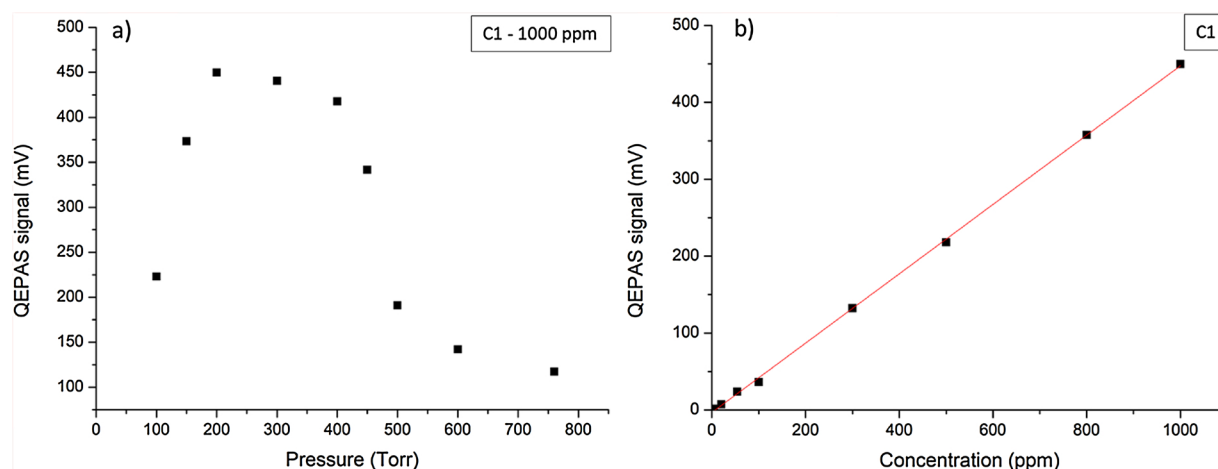


Fig. 3. a) $2f$ -signal peak values related to ν_3^{C1} at their optimum modulation depth for different pressures ranging from 100 Torr to atmospheric pressure; b) linearity of the $2f$ -signal peak values obtained at 200 Torr over a range of C1 concentrations from 4 ppm to 1000 ppm in pure N_2 .

current sinusoidal excitation and the QEPAS signal are out of phase. For this reason, the demodulation of the QEPAS signal occurs at a detection phase φ_i maximizing the demodulated signal amplitude. The main results from this investigation showed that by operating at an ICL temperature of 15 °C, the laser emission wavelength is resonant with the C_2H_6 absorption line located at 2986.25 cm^{-1} (ν_2^{C2}) at a laser current of $I = 65.5\text{ mA}$, while to target the strongest CH_4 absorption line peak at 2988.8 cm^{-1} (ν_3^{C1}) and for the C_2H_6 line located at 2990.1 cm^{-1} (ν_2^{C2}) the injected current must be set at $I = 48\text{ mA}$ and $I = 35\text{ mA}$, respectively. Thus, all three transitions ν_2^{C2} can be excited by keeping the laser operating temperature fixed at 15 °C and exploiting the ICL current dynamic range. Once the ICL operating conditions to target the selected CH_4 and C_2H_6 absorption lines were identified, the full sensor calibration procedure was performed. The QEPAS response to the excitation of ν_3^{C1} at different pressures was recorded. The data reported in Fig. 3a correspond to the $2f$ -QEPAS peak signals obtained by operating in the wavelength modulation configuration and optimizing the modulation depth for each different operating pressure. For methane the strongest response to photoacoustic excitation was achieved at a gas pressure of 200 Torr and a modulation amplitude of 130 mV peak-to-peak (V_{p-p}).

The detection phase φ_1 maximizing the QEPAS signal related to ν_3^{C1} excitation was 99.91° . These operating parameters were used for all the following C1 measurements.

Once determined the best operating conditions in terms of gas pressure and modulation depth, the $2f$ -signal peak signals at different C1 concentrations were recorded. Different CH_4 concentrations in the range 4–1000 ppm were generated, starting from a certified 1000 ppm CH_4 in N_2 mixture and using pure N_2 as diluting gas. By keeping fix the total flow of the mixture at 50 sccm, the uncertainty of the CH_4 concentration was estimated from the nominal values of the accuracy of the two mass flow meters, one dedicated to the methane and the other one to pure nitrogen. The error estimated for the minimum concentration level of 4 ppm of CH_4 is $\pm 1.6\text{ ppm}$.

The data reported in Fig. 3b demonstrate a good linearity for the CH_4 sensor over a wide range of concentrations from 4 ppm to 1000 ppm. A linearity coefficient of 0.46 mV/ppm was derived from the linear fit and a negligible intercept with $1-\sigma$ noise fluctuations of 0.073 mV .

In Fig. 4a and b are shown two representative acquisitions of CH_4 signal for 1000 ppm and 4 ppm, respectively.

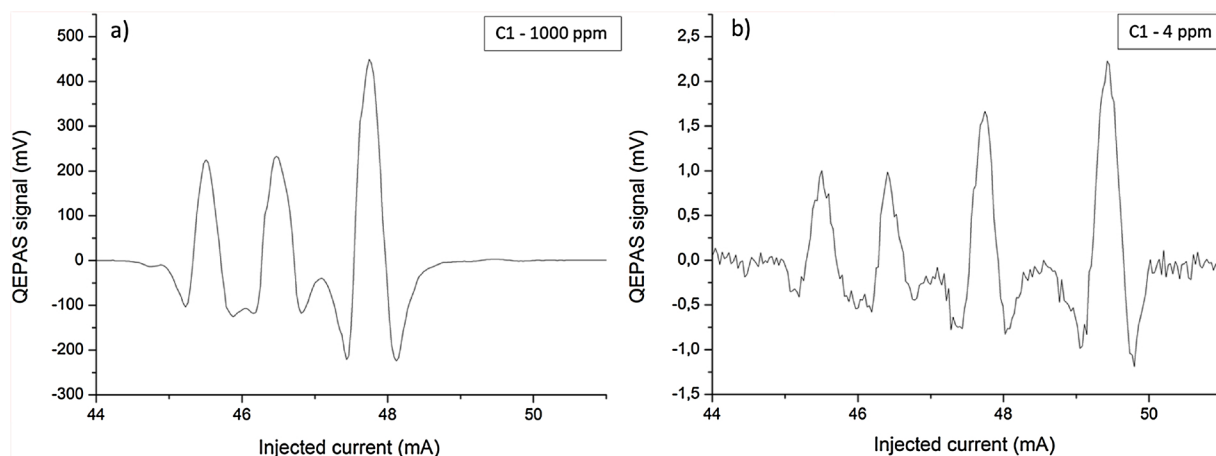


Fig. 4. a) $2f$ -signal corresponding to a humidified mixture of 1000 ppm-C1:N₂; b) $2f$ -signal corresponding to a humidified mixture of 4 ppm-C1:N₂.

In Fig. 4b it is clearly visible that a water absorption line falling at 2988.61 cm^{-1} [5], corresponding to at a laser injected current $I = 49.5\text{ mA}$, with a line strength of $1.1 \cdot 10^{-22}\text{ cm/mol}$, gives rise to a $2f$ -signal with a peak value of $\sim 2.25\text{ mV}$. This signal is barely visible in Fig. 4a due to the much higher CH₄ concentration. A very good correspondence between the absorption features listed in the Hitran database [13] and the $2f$ -QEPAS signal structures due to methane absorption was found. The background signal not involving gas absorption lines has comparable $1\text{-}\sigma$ noise fluctuations at different CH₄ concentrations. Allan deviation analysis [18] shows that for a 1 s integration time the detection limit for methane is $\sim 90\text{ ppb}$. This is a value well below the sensitivity needed for a sensor aimed at hydrocarbon detection at a well site, where C1 concentrations are expected to be generally well above the ppm scale.

5. Sensor calibration for ethane detection

Interesting results were observed when the sensor was calibrated for ethane detection. Line ν_2^{C2} was targeted for determining the sensitivity of the sensor with respect to C₂H₆. The calibration procedure for C₂H₆ is similar to the one illustrated in the previous section and the QEPAS response at different working pressures was investigated at a C₂H₆ concentration of 100 ppm. The optimum gas mixture pressure, located at 300 Torr, provides a QEPAS signal only ~ 1.3 times higher with respect to the value recorded at the atmospheric pressure (Fig. 5a), differently from methane where at 1 atm the QEPAS signal decreased by

$\sim 70\%$ with respect to the maximum signal recorded at 200 Torr. This means that the C₂H₆ sensor works efficiently also at atmospheric pressure which is advantageous for in-situ applications.

We observed that 200 Torr is the optimum working pressure for methane and the pressure controller has proven to have the smallest fluctuations at this pressure. Moreover, since the QEPAS signal at 200 Torr from ν_2^{C2} is $\sim 4\%$ smaller with respect to the highest signal recorded at 300 Torr (see Fig. 5a), a pressure of 200 Torr was chosen for performing the measurements for both CH₄ and C₂H₆. For C₂H₆ the optimum modulation depth results $V_{p-p} = 130\text{ mV}$ and detection phase $\varphi_2 = 166.15^\circ$. The C₂H₆-calibration curve is shown in Fig. 5b and the linearity of the QEPAS response was demonstrated from 100 ppm down to 2 ppm, with a linearity coefficient of 5.54 mV/ppm and a negligible intercept. Different from methane, ethane shows a broadband background absorption signal due to the presence of several absorption features with a small linewidth in the ICL operation spectral range. This can easily be noticed by comparing the signal at 1000 ppm for methane (see Fig. 4a) with the signal at 100 ppm for ethane (see Fig. 6a).

By comparing Fig. 6a and b, it can be noticed that the broadband background absorption levels off as the ethane concentration decreases. At 200 Torr and 2 ppm ethane concentration, the $1\text{-}\sigma$ signal value calculated far from the ν_2^{C2} $2f$ -peak is 0.14 mV , only about two times the noise level measured for a 1000 ppm CH₄:N₂ mixture. Allan deviation analysis [19] shows that for a 1 s integration time the detection limit for ethane is $\sim 7\text{ ppb}$. This represents a record for the QEPAS technique

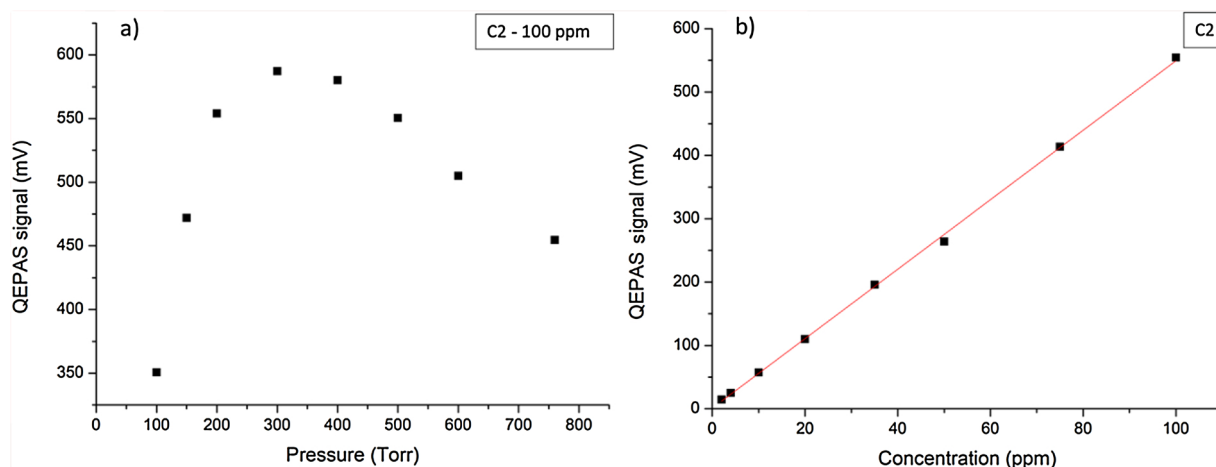


Fig. 5. a) $2f$ -signal peak values related to ν_2^{C2} at optimum modulation depths for different pressures, from 100 Torr to atmospheric pressure; b) linearity of the $2f$ -signal peak values obtained at 200 Torr for a range of C2 concentrations from 2 ppm to 100 ppm in pure N₂.

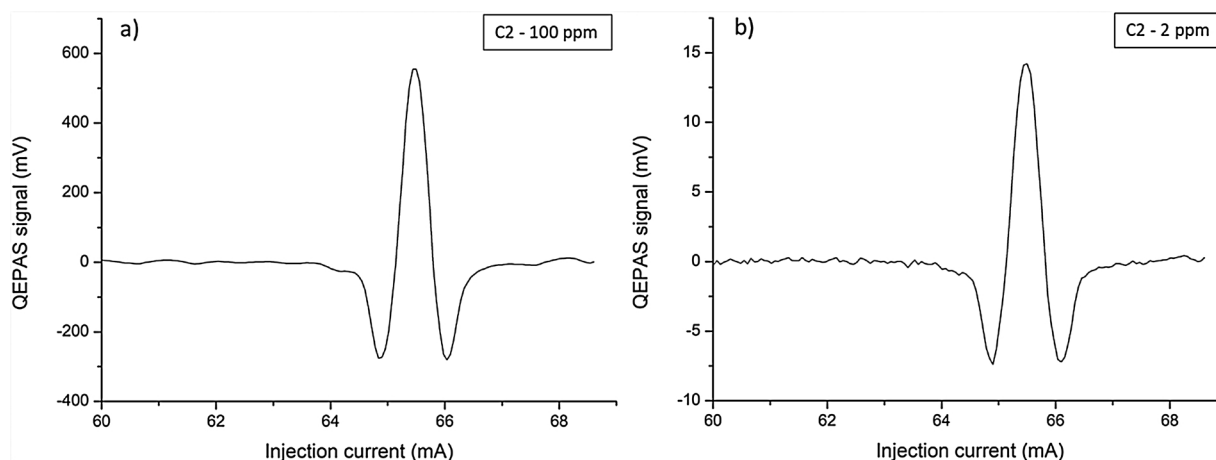


Fig. 6. a) 2f-signal corresponding to a humidified mixture of 100 ppm-C₂N₂; b) 2f-signal corresponding to a humidified mixture of 2 ppm-C₂N₂.

and opens the way to the implementation of QEPAS sensors for exploration and identification of ethane reservoirs, an application of strong interest for petrochemical and plastic industries.

6. Sensor performance and analysis of C1/C2 mixture

Considering the previous results, an unbalanced wet mixture containing 990 ppm CH₄, 10 ppm C₂H₆:N₂ was used to perform the first test of a fast C1/C2 detection scan. In the upper panel of Fig. 7, the QEPAS signal acquired for an ICL current span from 20 mA to 70 mA at T = 15 °C is displayed.

The working pressure was fixed at 200 Torr and the modulation amplitude at 130 mV_{p-p}. The second derivative profile of ethane absorption features ν_1^{C2} , ν_2^{C2} and the second derivative shape of the three-lines structure from methane are clearly visible. The spectral separation is coherent with the absorption cross-section graph for both CH₄ and C₂H₆ simulated using the Hitran database and shown in the lower panel of Fig. 7. In order to maximize the QEPAS response of the CH₄ and C₂H₆ lines, the optimal detection phases identified for each gas were used

during the current scan in the proximity of the related absorption features. A ν_3^{C1} 2f-signal peak of 455 mV and a ν_2^{C2} 2f-signal peak of 63 mV were obtained as expected from the sensor calibration. Furthermore, the full spectral scan over the ICL dynamic range showed the presence of barely visible water line at I = 59 mA, different from the one previously observed at I = 49.5 mA.

The detection scheme is versatile, because in one single current scan CH₄ and C₂H₆ can be independently detected at sub-ppm scale and can also deal with unbalanced mixtures in which the methane concentration is two orders of magnitude or even higher in concentration with respect to ethane. More interesting is a comparison between two or more broadband absorber molecules that can be found in downhole mixture compositions.

7. Propane detection and analysis of broadband absorbers spectra

In this section a detailed study of propane (C3) will be presented. In particular, consideration will be given on how its broadband spectrum interacts with the C2 background signal. Since propane absorption lines

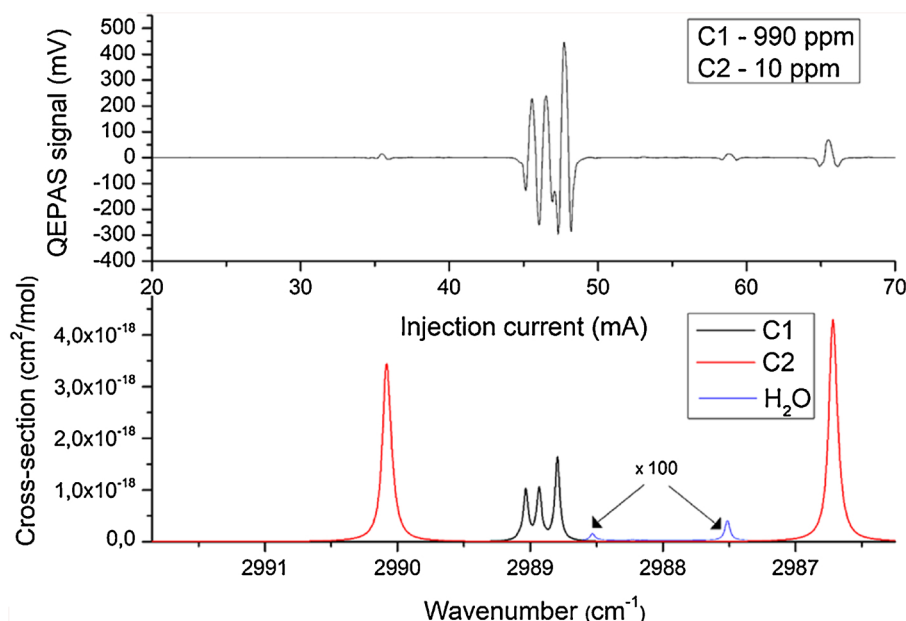


Fig. 7. Top panel: QEPAS 2f-signal for a humidified mixture of 990 ppm-C1 and 10 ppm-C₂N₂ with an adjusted detection phase of ν_3^{C1} (φ_1) and ν_2^{C2} (φ_2). Bottom panel: absorption cross-section for C1 and C2 obtained using the Hitran database [5]. Two weak H₂O absorption features are also shown (blue curve) by multiplying the related cross-sections by a factor of 100. (For interpretation of the references to colour in this figure legend, the reader is referred to the web version of this article).

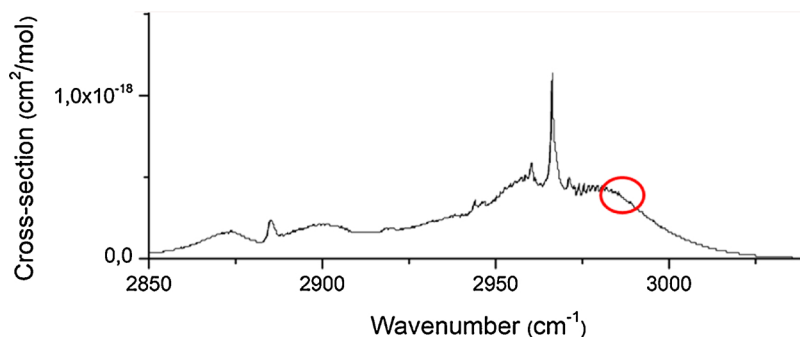


Fig. 8. Cross-section of propane in the range 2850–3100 nm, using PNNL database [20]. The red circle highlights the spectral range corresponding to the ICL tuning range. (For interpretation of the references to colour in this figure legend, the reader is referred to the web version of this article).

in the 2–4 μm range are not listed in the Hitran database, the PNNL database [20] was taken as reference to analyze the QEPAS measurements obtained for a mixture of 1000 ppm of $\text{C}_3\text{H}_8:\text{N}_2$. In Fig. 8 the absorption cross-section of C_3H_8 in the spectral range 2850–3100 nm is shown.

The C_3H_8 absorption cross-sections in the ICL tuning range (see the red circle in Fig. 8) are almost five times lower in linestrength than ν_2^{C2} ($1.26 \cdot 10^{-18} \text{ cm}^2/\text{mol}$) at atmospheric pressure. Nevertheless, the lack of sharp Lorentzian-like features like ν_2^{C2} or ν_3^{C1} leads to a photoacoustic excitation intensity in a wavelength modulation configuration that is low. In order to increase the C_3H_8 WM QEPAS signal, all the measurements were carried out at atmospheric pressure, where multiple absorption lines merge to build a spectrum composed of well-separated bands. The lock-in phase maximizing the C_3H_8 QEPAS signal was $\varphi_3 = 107.25^\circ$. In Fig. 9 the QEPAS spectra related to the C_3H_8 absorption bands spectra measured at atmospheric pressure and for different C_3H_8 dry concentrations, ranging from 1000 ppm to 200 ppm in pure N_2 , are plotted.

These spectra were obtained by scanning the laser injected current from 20 mA to 70 mA at $T = 15^\circ\text{C}$ and employing a modulation depth of 300 mVpp. Fig. 9b demonstrates the linearity of photoacoustic response as a function of the C_3H_8 concentration, extracted for the peak of the QEPAS spectrum ν_4^{C3} located at $I = 61.3 \text{ mA}$. The linearity coefficient is 0.0191 mV/ppm. The detection limit, extracted via an Allan deviation analysis of the QEPAS ν_4^{C3} peak signals, results in $< 3 \text{ ppm}$ for a 1 s integration time. It was verified that each peak of the C_3H_8 spectrum exhibits a linear QEPAS response with C3 concentrations, as observed in Fig. 9a). The QEPAS signal measured for a pure N_2 mixture

is flat within the ICL current dynamic range and comparable with the noise level. A flat background noise and QEPAS signal scaling linearly with the gas target concentration are mandatory requirements to compare C_2H_6 and C_3H_8 backgrounds. The QEPAS signal $Y(\lambda)$ acquired for a mixture of n gases (C_2H_6 and C_3H_8) for a given wavelength spectrum can be assumed to be the sum of the QEPAS signals related to the individual gases:

$$Y(\lambda) = \sum_{i=0}^n A_i X(\lambda)_i = A_2 X(\lambda)_{C2} + A_3 X(\lambda)_{C3} \quad (1)$$

where $Y(\lambda)$ is the acquired QEPAS signal (in mV), A_i is the concentration of the i -th gas (in ppm) and X_i the related QEPAS spectrum, in mV/ppm unit [21]. If the operating temperature is set to 15°C , the laser emission wavelength is related to the drive current. In order to discriminate both contributions in C2-C3 mixtures, an injected current range from 35 to 60 mA was selected, in which range no strong C_2H_6 features are present and both C_2H_6 and C_3H_8 absorption broadband backgrounds can be easily compared (see Fig. 10a). The detection phase used for these measurements is the one maximizing the C3 QEPAS signal, i.e., $\varphi_3 = 107.25^\circ$: in this way we also slightly reduced the intensity of the C2 background signal. However, it was verified that the C2 background signal detected at φ_3 is still linear as function of C2 concentrations. The reference QEPAS spectra used for the fitting procedure using Eq. 1 are the C_2H_6 and C_3H_8 signals recorded at 1000 ppm in pure N_2 concentration, therefore Eq. 1 becomes:

$$Y = a X_{1\%}^{C2} + b X_{1\%}^{C3} \quad (2)$$

where a and b are the fraction of 1000 ppm of the reference spectra. The first validation test of this multi-gas detection approach was made using

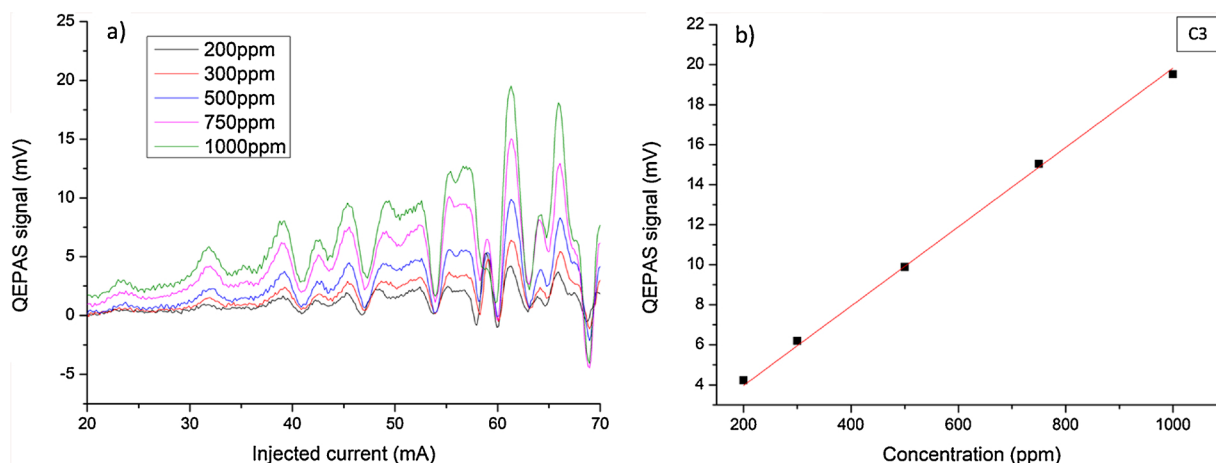


Fig. 9. a) 2f-QEPAS spectra measured for different C3 concentrations from 1000 ppm to 200 ppm in pure N_2 at atmospheric pressure and using a modulation depth $V_{p-p} = 300 \text{ mV}$, in the laser current range 20–70 mA; b) linear fit (red line) of the 2f-signal peak values (black square dots) related to the absorption feature falling at $I = 61.3 \text{ mA}$ for a range of C3 concentrations from 1000 ppm to 200 ppm. (For interpretation of the references to colour in this figure legend, the reader is referred to the web version of this article).

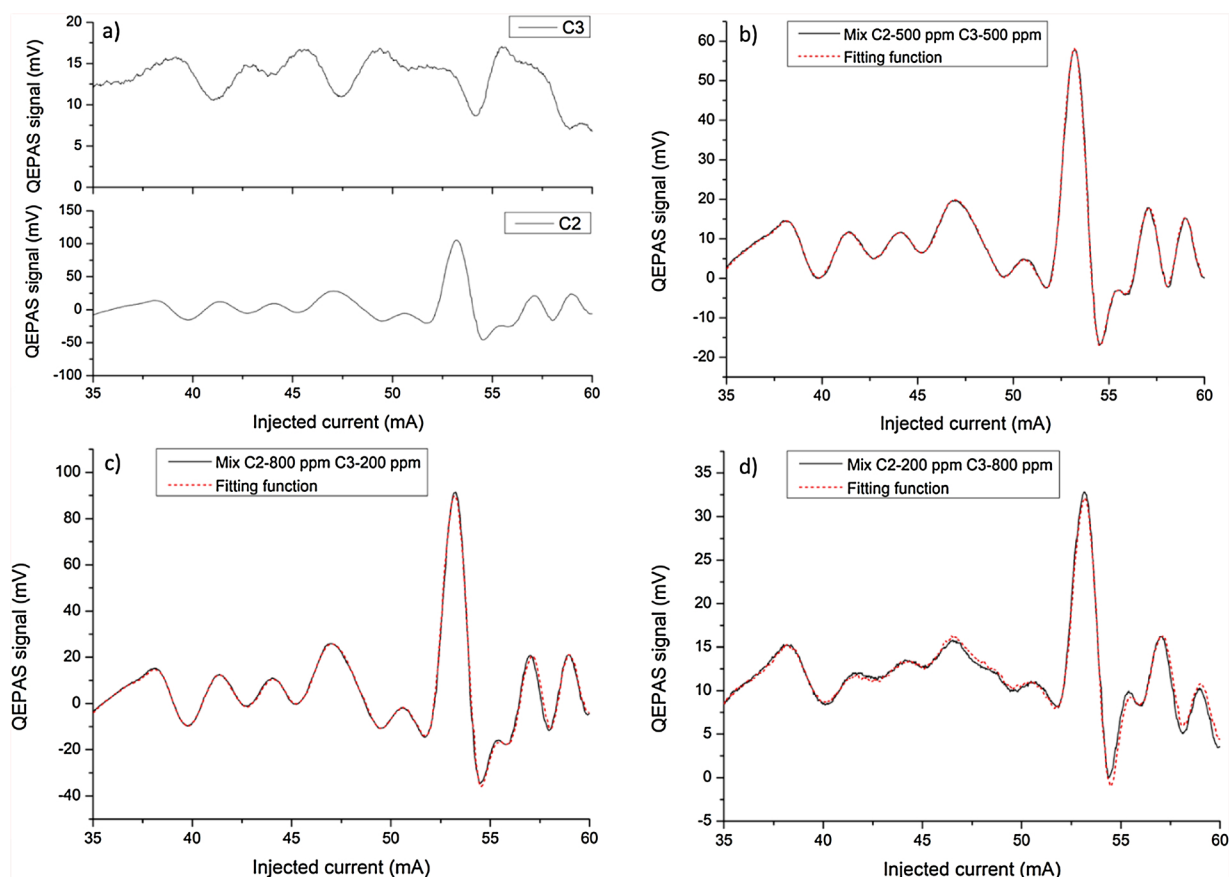


Fig. 10. a) Top panel: 2f-signal for 1000 ppm-C3:N₂ acquired in the laser injected current range 35–60 mA. Bottom panel: 2f-signal for 1000 ppm-C2:N₂; b) 2f-signal for a dry mixture containing 500 ppm of C2 and 500 ppm of C3, in pure N₂; c) 2f-signal for a dry mixture containing 800 ppm of C2 and 200 ppm of C3 in pure N₂; d) 2f-signal for a dry mixture containing 200 ppm of C2 and 800 ppm of C3 in pure N₂.

dry mixtures composed of: i) C2-500 ppm, C3-500 ppm in pure N₂ (mix#1); ii) C2-800 ppm, C3-200 ppm in pure N₂ (mix#2); iii) C2-200 ppm, C3-800 ppm in pure N₂ (mix#3).

In Fig. 10b–d the QEPAS spectra and the related fits for all the three gas mixtures are shown. The calculated concentration values are listed in Table 1. In brackets the 95% confidence interval uncertainties are reported.

The differences between the fitting parameters, i.e. the calculated C₂H₆ and C₃H₈ concentrations, and the nominal concentrations expected remains below 5% and are mainly due to uncertainties in the certified gases flows used for producing the mixtures (especially for flows as low as 8 sccm, as used in our experiments). The obtained results successfully demonstrate the feasibility to perform photoacoustic C2/C3 gas detection by fitting the QEPAS spectra measured for the gas mixtures. Among different valid approaches such as multivariate analysis or machine learning, a fitting procedure based on a linear combination of reference spectra still represents the most straightforward strategy. Since in the investigated spectral range, C1 is characterized by well isolated absorption peaks and no background, we successfully determined CH₄, C₂H₆ and C₃H₈ concentrations in humidified and dry gas mixtures respectively, using pure nitrogen as gas carrier. The next

step will be a detailed investigation of C1/C2/C3 mixtures in a large dynamic range of concentration from several % to few ppb. Subsequently, butane will be added to the gas mixture in order to analyze gas samples as similar as possible to the natural gas composition. All these tasks aim to monitor natural gas sample compositions in situ and in real time for petrochemical applications.

8. Conclusions

Hydrocarbon concentration monitoring is essential for the oil & gas industry and the possibility to measure in real time methane and ethane as well as propane concentrations will represent a breakthrough for estimating reserves and assist in petrochemical exploration and drilling. In this paper, we demonstrated that a QEPAS sensor is capable of simultaneous detection of methane, ethane and propane using a single ICL source operating around 3.3 μm. The QEPAS sensor achieved an ultimate detection limit of 90 ppb, 7 ppb and 3 ppm for CH₄, C₂H₆ and C₃H₈, respectively, for a 1 s integration time. Propane has never been detected previously using QEPAS and the detection limit achieved for ethane represents a record value for the QEPAS technique [22]. We also demonstrated the possibility to detect CH₄, C₂H₆ and C₃H₈ at

Table 1
Actual and calculated C₂H₆ and C₃H₈ concentration for the investigated gas mixtures.

Mixture	Actual C ₂ H ₆ concentration [ppm]	Actual C ₃ H ₈ concentration [ppm]	Calculated C ₂ H ₆ concentration [ppm]	Calculated C ₃ H ₈ concentration [ppm]
1	500	500	487.02 (± 1.4)	520.00 (± 2.5)
2	800	200	828.98 (± 3.8)	208.01 (± 6.8)
3	200	800	199.98 (± 1.7)	831.47 (± 2.9)

atmospheric pressure, thereby avoiding the use of pressure controller systems. Further improvements will be achieved by implementing new generations of QTFs [23], overtone modes operation [24,25] and new micro-resonator systems [26,27]. The final goal will be the development of a QEPAS sensor capable to perform CH₄, C₂H₆ and C₃H₈ real-time measurement for upstream, midstream and downstream petrochemical sectors, and achieve the capability to detect butane.

Acknowledgements

The authors from Dipartimento Interateneo di Fisica di Bari acknowledge the financial support from THORLABS GmbH, within the joint-research laboratory PolySense. Frank K. Tittel acknowledges the support by the Welch Foundation under Grant No. C0568.

References

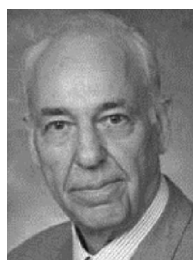
- [1] J. Meyer, I. Vurgaftman, Quantum and interband cascade lasers, *Opt. Eng.* 49 (2010) 111101.
- [2] I. Vurgaftman, R. Wei, M. Kamp, J.R. Meyer, C.L. Canedy, C.S. Kim, N. Kim, W.W. Bewley, C.D. Merritt, J. Abell, S. Höfling, Interband Cascade Lasers, *J. Phys. D Appl. Phys.* 48 (2015) 12.
- [3] C. Zheng, W. Ye, N.P. Sanchez, A.K. Gluszek, A.J. Hudzikowski, C. Li, L. Dong, R.J. Griffin, F.K. Tittel, Infrared dual-gas CH₄/C₂H₆ sensor using two continuous-wave interband cascade lasers, *IEEE Photonics Technol. Lett.* 28 (2016) 2351.
- [4] L. Dong, F.K. Tittel, C. Li, N.P. Sanchez, H. Wu, C. Zheng, Y. Yu, A. Sampaolo, R.J. Griffin, "Compact TDLAS based sensor design using interband cascade lasers for mid-IR trace gas sensing," *Opt. Exp.* 24 (2016) A528.
- [5] L.S. Rothman, I.E. Gordon, Y. Babikov, A. Barbe, D. Chris Benner, P.F. Bernath, M. Birk, L. Bizzocchi, V. Boudon, L.R. Brown, A. Campargue, K. Chance, E.A. Cohen, L.H. Coudert, V.M. Devi, B.J. Drouin, A. Fayt, J.M. Flaud, R.R. Gamache, J.J. Harrison, J.M. Hartmann, C. Hill, J.T. Hodges, D. Jacquemart, A. Jolly, J. Lamouroux, R.J. Le Roy, G. Li, D.A. Long, O.M. Lyulin, C.J. Mackie, S.T. Massie, S. Mikhailenko, H.S.P. Muller, O.V. Naumenko, A.V. Nikitin, J. Orphal, V. Perevalov, A. Perrin, E.R. Polovtseva, C. Richard, M.A.H. Smith, E. Starikova, K. Sung, S. Tashkun, J. Tennyson, G.C. Toon, V.G. Tyuterev, G. Wagner, J. Quant. Spectrosc. Radiat. Transf. 130 (2013) 4–50.
- [6] J.G. Speight, *The Chemistry and Technology of Petroleum*, CRC Press, Boca Raton, 2014.
- [7] V. Spagnolo, P. Patimisco, S. Borri, G. Scamarcio, B.E. Bernacki, J. Kriesel, Part-per-trillion level SF₆ detection using a quartz enhanced photoacoustic spectroscopy based sensor with single-mode fiber-coupled quantum cascade laser excitation, *Opt. Lett.* 37 (2012) 460.
- [8] P. Patimisco, G. Scamarcio, F.K. Tittel, V. Spagnolo, Quartz-enhanced photoacoustic spectroscopy: a review, *Sensors* 14 (2014) 6165.
- [9] P. Patimisco, A. Sampaolo, L. Dong, F.K. Tittel, V. Spagnolo, Recent advances in quartz enhanced photoacoustic sensing, *Appl. Phys. Rev.*, *Appl. Phys. Rev.* 5 (2018) 011106.
- [10] A.A. Kosterev, F.K. Tittel, D. Serebryakov, A. Malinovsky, A. Morozov, Applications of quartz tuning fork in spectroscopic gas sensing, *Rev. Sci. Instrum.* 76 (2005) 043105.
- [11] A. Sampaolo, P. Patimisco, M. Giglio, L. Chieco, G. Scamarcio, F.K. Tittel, V. Spagnolo, Highly sensitive gas leak detector based on a quartz-enhanced photoacoustic SF₆ sensor, *Opt. Exp.* 24 (2016) 15872–15881.
- [12] M. Jahjah, W. Kiang, N.P. Sanchez, W. Ren, P. Patimisco, V. Spagnolo, S.C. Herndon, R.J. Griffin, F.K. Tittel, Atmospheric CH₄ and N₂O measurements near Greater Houston area landfills using QCL-based QEPAS sensor system during DISCOVERY-AQ 2013, *Opt. Lett.* 39 (2014) 957.
- [13] P. Patimisco, A. Sampaolo, H. Zheng, L. Dong, F.K. Tittel, V. Spagnolo, "Quartz enhanced photoacoustic spectrophones exploiting custom tuning forks: a review," *Adv. Phys. X* 2 (2016) 169–187.
- [14] H. Wu, L. Dong, H. Zheng, Y. Yu, W. Ma, L. Zhang, W. Yin, L. Xiao, S. Jia, F.K. Tittel, Beat frequency quartz-enhanced photoacoustic spectroscopy for fast and calibration-free continuous trace-gas monitoring, *Nat. Comm.* 8 (2017) 15331.
- [15] S. Böttger, M. Köhring, U. Willer, W. Schade, Off-beam quartz-enhanced photoacoustic spectroscopy with LEDs, *Appl. Phys. B* 113 (2013) 227.
- [16] V. Spagnolo, P. Patimisco, R. Pennetta, A. Sampaolo, G. Scamarcio, M.S. Vitiello, F.K. Tittel, THz Quartz-enhanced photoacoustic sensor for H₂S trace gas detection, *Opt. Exp.* 23 (2015) 7574.
- [17] A. Sampaolo, P. Patimisco, M. Giglio, M.S. Vitiello, H.E. Beere, D.A. Ritchie, G. Scamarcio, F.K. Tittel, V. Spagnolo, Improved tuning fork for terahertz quartz-enhanced photoacoustic spectroscopy, *Sensors* 16 (2016) 439.
- [18] P. Patimisco, A. Sampaolo, Y. Bidaux, A. Bismuto, M. Schott, J. Jiang, A. Muller, J. Faist, F.K. Tittel, V. Spagnolo, Purely wavelength- and amplitude-modulated quartz-enhanced photoacoustic spectroscopy, *Opt. Exp.* 24 (2016) 25943.
- [19] M. Giglio, P. Patimisco, A. Sampaolo, G. Scamarcio, F.K. Tittel, V. Spagnolo, Allan Deviation Plot as a tool for quartz-enhanced photoacoustic sensors noise analysis, *IEEE Trans. Ultrason. Ferroelect. Freq. Control.* 63 (2016) 555.
- [20] <http://vpl.astro.washington.edu/spectra/>.
- [21] I.T. Sorokina, K.L. Vodopyanov, *Solid-State Mid-Infrared Laser Sources*, Springer-Verlag, Berlin Heidelberg, 2003.
- [22] C. Li, L. Dong, C. Zheng, J. Lin, Y. Wang, F.K. Tittel, Pbpy-level ethane detection using quartz-enhanced photoacoustic spectroscopy with a continuous-wave, room temperature interband cascade laser, *Sensors* 18 (2018) 723.
- [23] P. Patimisco, A. Sampaolo, L. Dong, M. Giglio, G. Scamarcio, F.K. Tittel, V. Spagnolo, Analysis of the electro-elastic properties of custom quartz tuning forks for photoacoustic gas sensing, *Sens. Act. B Chem.* 227 (2016) 539.
- [24] F.K. Tittel, A. Sampaolo, P. Patimisco, L. Dong, A. Geras, T. Starecki, V. Spagnolo, Analysis of overtone flexural modes operation in quartz-enhanced photoacoustic spectroscopy," *Opt. Exp.* 24 (2016) A682.
- [25] A. Sampaolo, P. Patimisco, L. Dong, A. Geras, G. Scamarcio, T. Starecki, F.K. Tittel, V. Spagnolo, Quartz-enhanced photoacoustic spectroscopy exploiting tuning fork overtone modes, *Appl. Phys. Lett.* 107 (2015) 231102.
- [26] H. Zheng, L. Dong, A. Sampaolo, H. Wu, P. Patimisco, X. Yin, W. Ma, L. Zhang, W. Yin, V. Spagnolo, S. Jia, F.K. Tittel, Single-tube on-beam quartz-enhanced photoacoustic spectroscopy, *Opt. Lett.* 41 (2016) 978.
- [27] H. Zheng, L. Dong, A. Sampaolo, P. Patimisco, W. Ma, L. Zhang, W. Yin, L. Xiao, V. Spagnolo, S. Jia, F.K. Tittel, Overtone resonance enhanced single-tube on-beam quartz enhanced photoacoustic spectrophone, *Appl. Phys. Lett.* 109 (2016) 111103.



Pietro Patimisco obtained the Master degree in Physics (cum laude) in 2009 and the PhD Degree in Physics in 2013 from the University of Bari. Since 2013, he is a Post-Doctoral Research associate at the University of Bari. He was a visiting scientist in the Laser Science Group at Rice University in 2013 and 2014. Dr. Patimisco's scientific activity addressed both micro-probe optical characterization of semiconductor optoelectronic devices and photoacoustic gas sensors. Recently, his research activities included the study and applications of trace-gas sensors, such as quartz-enhanced photoacoustic spectroscopy and cavity enhanced absorption spectroscopy in the mid infrared and terahertz spectral region, leading to several publications, including a cover paper in *Applied Physics Letter* of the July 2013 issue.



Angelo Sampaolo obtained his Master degree in Physics in 2013 and the PhD Degree in Physics in 2017 from the University of Bari. He was a visiting researcher in the Laser Science Group at Rice University in 2016 and 2017. Since May 2017, he is a Post-Doctoral Research associate at the University of Bari. His research activity has included the study of the thermal properties of heterostructured devices via Raman spectroscopy. Most recently, his research interest has focused on the development of innovative techniques in trace gas sensing, based on Quartz Enhanced Photoacoustic Spectroscopy and covering the full spectral range from near-IR to THz. His achieved results have been acknowledged by a cover paper in *Applied Physics Letter* of the July 2013 issue.



Frank K Tittel obtained his bachelor, master, and doctorate degrees in physics from the University of Oxford in 1955 and 1959, respectively. From 1959 to 1967, he was a Research Physicist with General Electric Research and Development Center, Schenectady, New York. Since 1967 he has been on the faculty of the Department of Electrical and Computer Engineering and Biomedical Engineering at Rice University in Houston, TX, where he currently an Endowed Chaired Professor. Current research interests include various aspects of quantum electronics, in particular laser spectroscopy and laser applications in environmental monitoring, atmospheric chemistry, industrial process control, and medical diagnostics. Dr. Tittel is a Fellow of the IEEE, Optical Society of America, the American Physical Society and SPIE.



Vincenzo Spagnolo obtained the PhD in physics in 1994 from University of Bari. From 1997 to 1999, he worked as researcher of the National Institute of the Physics of Matter (INFN). Since 2004, he works at the Technical University of Bari, formerly as assistant professor and, starting from 2015, as associate Professor of Physics. He is the director of the joint-research lab PolySense created by Technical University of Bari and THORLABS GmbH. His research interests include optoacoustic gas sensing and spectroscopic techniques for real-time device monitoring. His research activity is documented by more than 160 publications and two filed patents. He has given more than 40 invited presentations at international conferences and workshops.

Prof. Spagnolo is senior member of the SPIE and senior member of OSA.



Marilena Giglio received the M.S. degree (cum laude) in Applied Physics from University of Bari, Italy, in 2014, discussing the results obtained during a five months internship at the Academic Medical Center of Amsterdam, The Netherlands. Since 2014, she is pursuing a post-degree master in mechatronics and is currently a Research Assistant in the Physics Department of the University of Bari. Her research activity has included Optical Coherence Tomography (OCT) as an imaging technique for thin tissues and the analysis of the parameters of speckle distribution in OCT B-scans. Recently, her research activity has focused on the development of gas sensors based on Quartz-Enhanced Photoacoustic Spectroscopy.